



Optical $n(p, T_{90})$ Measurement Suite 3: Results at $\lambda = 1542$ nm

Patrick F. Egan¹ · Yuanchao Yang²

Received: 2 July 2024 / Accepted: 18 July 2024

This is a U.S. Government work and not under copyright protection in the US; foreign copyright protection may apply 2024

Abstract

Single-isotherm $n(p, T_{90})$ results are reported for the gases Ar, N₂, H₂O, and D₂O at vacuum wavelength $\lambda = 1542.383(1)$ nm. The argon and nitrogen isotherms were measured near 303 K; the water isotherms were measured near 373 K. Combined with the two previous articles of this series, the present results beget several insights via dispersion analyses. The argon result is highly consistent with static measurement plus *ab initio* calculation of dispersion polarizability. The nitrogen result is nominally consistent with one recent experiment and the dipole oscillator strength distributions, but the present work offers a refined estimate of the molar refractivity at optical wavelengths. For ordinary and heavy water, the dispersion trend is nominally consistent with existing liquid measurements. However, water's absorption features in the near-infrared preclude a reliable comparison of the present result with literature.

Keywords Dispersion · Polarizing gas thermometry · Refractometry · Thermodynamic metrology

1 Introduction

Imminent commercial optical pressure standards might find it most practical to operate at telecom wavelength. Over the past few decades, the telecom industry has innovated much gadgetry in the C-band infrared (1530 nm to 1565 nm). For precision measurement, the bane of telecom wavelength has been the absence of turnkey narrow linewidth lasers (sub-kilohertz). In today's market, narrow linewidth solutions are provided by at least three technologies: fiber ring resonators, diode lasers with an external waveguide Bragg reflector, and whispering gallery mode resonators. As

✉ Patrick F. Egan
egan@nist.gov

¹ National Institute of Standards and Technology, Gaithersburg, MD 20899, USA

² National Institute of Metrology, Beijing 100029, China

a candidate source for an optical pressure standard, a HeNe laser tube might offer the better tradeoff between narrow linewidth and cost; however, telecom photonics probably have the advantage from the total system perspective (fiber-hardened, plug-and-play, and so on). Most importantly, telecom lasers also have the multi-gigahertz tunability essential for miniaturization (i.e., centimeter-scale optical cavities).

The optical pressure scale [1] $p_{\text{ops}} = \frac{2RT}{3A_{\text{R}}}(n - 1) + \dots$ is realized by measurement of refractivity $n - 1$ at known temperature T , with R being the molar gas constant. An optical pressure standard therefore comprises an accurate refractometer and thermometer. The key parameter to the realization is the molar refractivity $A_{\text{R}} = A_{\text{e}}(0) + \Delta A_{\text{e}}(\omega) + A_{\text{m}}$, in which the electronic contribution A_{e} is about five orders of magnitude larger than the magnetic A_{m} , and $\frac{\Delta A_{\text{e}}(\omega)}{A_{\text{e}}(0)} \approx 1\%$ for visible wavelength. For practical metrology gases like nitrogen and argon, the most accurate knowledge about A_{R} comes from measurement. Until now, measurements have either provided zero frequency $A_{\text{e}}(0)$ by dielectric constant, $A_{\text{R}}(0)$ by microwave refractive index, or $A_{\text{R}}(\omega)$ at 633 nm by optical refractive index. Knowledge about A_{R} in the C-band infrared is limited. Consequently, an optical pressure standard operating at the (arguably) more commercially viable telecom wavelengths does not have a solid metrological foundation.

This article is the final installment in a three-part series. It extends the previous two articles [2, 3] by reporting single-isotherm $n(p, T_{90})$ results at $\lambda = 1542.383(1)$ nm for Ar, N₂, H₂O, and D₂O. All background concepts and analysis details are in the previous two articles. Here, the pivotal difference is the change in operating wavelength. Consequently, this article is brief, and just reports the optical setup, and then places the key result (molar refractivity A_{R}) in the literature context.

2 Setup

A schematic of the optical setup is shown in Fig. 1. The 1542 nm system of Fig. 1 has two main differences over the 633 nm system of Refs. [2, 3]: (1) a frequency comb referenced to the SI second via GPS was used as the frequency reference (instead of a iodine-stabilized laser), and (2) an external cavity diode laser was used for locking to the resonance frequency of the Fabry–Perot (FP) cavity (instead of a HeNe laser tube). More details and photographs of the equipment are given in the supplemental material

The diode laser employed has feedback provided by a Bragg reflector inside its butterfly package. [In optics, “butterfly package” is standard usage. It refers to a metal housing about $(25 \times 15 \times 8)$ mm³, with 14 electrical control pins projecting from the sides and a fiber optic output from one end. The diode laser chip, thermoelectric cooler, thermistor, Bragg reflector, isolator, and fiber coupling optics are all monolithically assembled inside the housing.] The free-running laser has a specified linewidth of 2 kHz. Noise on the drive current was minimized by limiting its bandwidth to 100 Hz. The operating wavelength was chosen to overlap with an accurately known absorption feature of acetylene. The concept was to operate

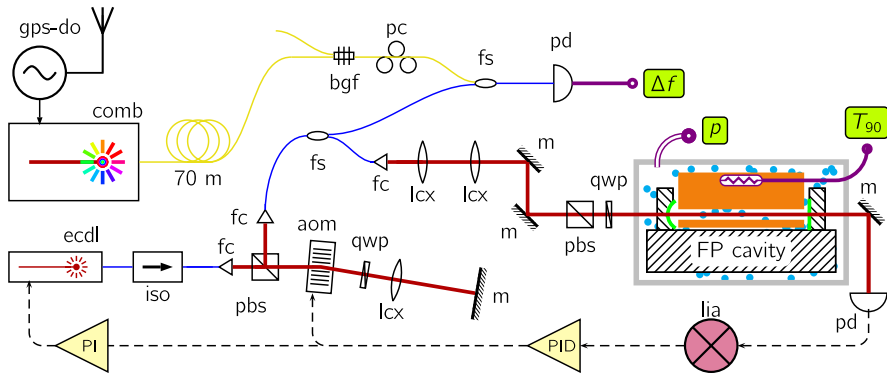


Fig. 1 Optical setup for the $\lambda = 1542$ nm results. Components include external cavity diode laser (ecdl), isolator (iso), fiber coupler/collimator (fc), polarizing beamsplitter (pbs), acousto-optic modulator (aom), quarter-waveplate (qwp), convex lens (lcx), mirror (m), fiber splitters (fs), global positioning system disciplined oscillator (gps-do), Bragg grating filter (bgf), polarization controller (pc), photodetector (pd), and lock-in amplifier (lia)

with an acetylene-stabilized laser frequency reference, which is a portable device. However, the use of the frequency comb has made acetylene wavelength a moot point. (The frequency comb is in a separate space to the refractometry lab, and supplies the optical reference frequency over 70 m of fiber optic cable.)

The configuration (Fig. 1) to lock the laser to the FP cavity resonance is similar to the HeNe setup. Fast (16 kHz) frequency control was provided by a doublepass acousto-optic modulator; in series with the fast loop, slow (1 Hz) frequency control was provided by the thermoelectric cooler inside the butterfly package. The hysteresis-free tuning range of the laser is about 8 GHz. In this work, the voltage applied to the thermoelectric cooler was circuit limited so that frequency only tuned 1.2 GHz, or 20 % wider than the free spectral range of the cavity. The modulation and analog control electronics were identical to the HeNe setup.

The FP cavity was the same as Refs. [2, 3]. The mirrors that form the cavity were dual-coated for 633 nm and 1542 nm wavelengths. The finesse at 1542 nm was estimated as 3200, which is about 13 % higher than the value at 633 nm. (Finesse was estimated by measurements of the free spectral range divided by the full-width half-maximum transmission linewidth.) The mirror parameter ϵ_r of Eq. (1) in Ref. [2] differs by about 14 % between the wavelengths, and has negligible influence on the results.

The previous paragraph is emphasized: the same FP cavity has been used in Refs. [2, 3] and the present work. This fact means that dominating errors related to cavity length have little influence on relative results between wavelengths. For argon and nitrogen, the dominating length error is cavity compressibility, which would be identical at both wavelengths. For water vapor, the dominating length error is the moisture-dependent reflection phase shift from the cavity mirrors. This error is chromatic, but as explained below, the wavelength dependence is small (and compensated), and is further diminished by the choice of operating temperature.

3 Results

For argon and nitrogen, single isotherms at 303 K were acquired with a procedure identical to Ref. [2]—nineteen set pressures up to 500 kPa generated by a piston gage. For ordinary and heavy water, single isotherms at 373 K were acquired with a procedure identical to Ref. [3]—ten set pressures below 2 kPa measured with a calibrated pressure transducer.

The molar refractivities deduced for all four gases are listed in Table 1. Next follows some discussion, placing the results in the literature context. Dispersion in all four gases will be discussed in terms of $\delta A_R \equiv A_{\text{meas}} - A_{\text{ref}}$, referenced to zero frequency and with

$$A_{\text{ref}} = A_e(0) + \Delta A_e(\omega) + A_\mu. \quad (1)$$

The literature sources used for static polarizability $A_e(0)$, dispersion polarizability $\Delta A_e(\omega)$, and diamagnetic susceptibility A_μ are specified for each gas below. (All literature uses atomic units for angular frequency ω . This work describes all parameters related to A_R in SI units.)

Unless otherwise stated, all uncertainties in this work are one standard uncertainty, corresponding to approximately a 68 % confidence level.

3.1 Discussion about Ar and N₂

At 303 K, the uncertainty of the argon and nitrogen results is $3 \times 10^{-6} \cdot A_R$, and operation at 1542 nm incurs no additional uncertainty over what is detailed in Ref. [2]. The uncertainty is dominated by the knowledge of the generated pressure (1.9 $\mu\text{Pa}/\text{Pa}$) [4], and to a lesser extent knowledge of the thermometry error $T - T_{90}$ (1.1 $\mu\text{K}/\text{K}$) [5].

3.1.1 Argon

The single-isotherm $n(p, T_{90})$ data for argon are plotted in Fig. 2a. The subplot is in a conventional format, showing molar refraction as a function of density. The

Table 1 Results for molar refractivity at $\lambda = 1542.383(1)$ nm from the present work, and at $\lambda = 632.9908(1)$ nm from the same apparatus [2, 3]

Gas	$A_R/(\text{cm}^3/\text{mol})$	
	$\lambda = 1542.383$ nm	$\lambda = 632.9908$ nm
Ar	4.149749(13)	4.195735(13)
N ₂	4.396718(14)	4.446175(14)
H ₂ O	3.6689(18)	3.7470(18)
D ₂ O	3.6400(18)	3.7146(18)

Argon and nitrogen measured at $T = 303$ K; ordinary and heavy water measured at $T = 373$ K. Numbers in parentheses denote standard uncertainty

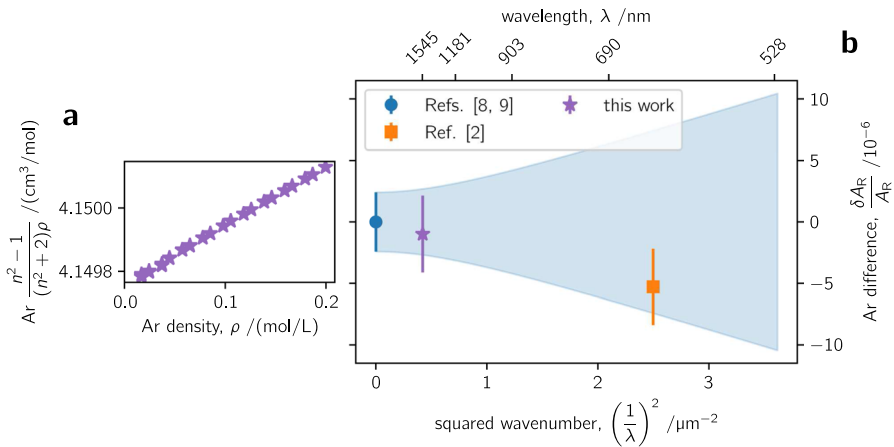


Fig. 2 (a) Single-isotherm results for argon at 1542 nm and 303 K. (b) Dispersion analysis plotted as relative difference from the reference value; the shaded area is an estimate of uncertainty on the reference value. Errorbars span the uncertainty of the cited literature

deviation from constant molar refraction is primarily due to the second refractivity virial coefficient. Extracting information about this coefficient from the data is dubious: it requires very accurate knowledge about the compressibility factor, which would ultimately use previous data from this apparatus at a different wavelength [2]. In short, the deduction would be circular: two conflated nonlinear coefficients would be inferred from the same data. (The difference in the second refractivity virial coefficient [6] between 633 nm and 1542 nm is far too small for these measurements to say anything about the frequency dependence.)

In principle, extrapolating Fig. 2a to zero density obtains the molar refraction. However, the A_R in Table 1 was determined by the more appropriate method of single-isotherm refractive-index gas thermometry [7]. The method fit the (isothermal) generated pressure to a power series of refractivity $p = (n - 1)\mathcal{A}[1 + (n - 1)\mathcal{B} + (n - 1)^2\mathcal{C}] + \epsilon_p$, and $A_R = \frac{2RT}{3\mathcal{A}}$ was extracted from the linear refractivity term. This analysis circumvents the nonlinear influences from the density and refractivity virial coefficients. The implementation used total least squares, with the refractivity and pressure weighted by the squared reciprocal of their respective uncertainties. The identified $\epsilon_p = -1.4$ mPa influences the final result at the level of $1 \times 10^{-7} \cdot A_R$. It is emphasized that ϵ_p is a physically justified parameter, and past experience [2] corroborates that its inclusion in the single-isotherm regression produces a final A_R closer to true value (multi-isotherm regression).

The argon result at 1542 nm is shown in the literature context by the dispersion plot of Fig. 2b. The reference value of (1) follows the recommendation of Lesiuk and Jeziorski [8]: $A_e(0)$ is due to the highly accurate capacitance measurement of Gaiser and Fellmuth [9], $\Delta A_e(\omega)$ uses the ω^6 -order Cauchy equation from the *ab initio* calculation of Lesiuk and Jeziorski [8], and A_μ is from the *ab initio* calculation for diamagnetic susceptibility, also due to Lesiuk and Jeziorski [10]. The uncertainty

on the reference value has $2.4 \times 10^{-6} \cdot A_R$ from the static measurement, and 0.05 % on the first Cauchy coefficient, which translates into $1.2 \times 10^{-6} \cdot A_R$ at 1542 nm. (The magnetic uncertainty contribution is probably negligible, but a solution to the susceptibility puzzle [10] needs a new experimental development.)

It is clear from Fig. 2b that all results for argon are highly consistent. The two optical results have been produced by the same apparatus (but separated in time by 18 months), and extrapolate very close to the zero frequency result of Gaiser and Fellmuth [9]. In the context of an optical pressure scale, the optical properties of argon are on solid ground.

[Two other notable static results are not shown in Fig. 2b. The first is the *ab initio* calculation of Lesiuk and Jeziorski [8], which has $\frac{\delta A_R}{A_R} = (2.8 \pm 17) \times 10^{-5}$, and is consistent with A_{ref} within the mutual standard uncertainty. The second static result not shown is the older capacitance measurement of Schmidt and Moldover [11], which has $\frac{\delta A_R}{A_R} = (32.4 \pm 4.5) \times 10^{-5}$, and is inconsistent with A_{ref} by seven times the mutual standard uncertainty. The work of Schmidt and Moldover is relevant for the nitrogen discussion below. Finally, a refractivity measurement at 800 nm due to Zhang et al. [12] has $\frac{\delta A_R}{A_R} = (27.2 \pm 2.3) \times 10^{-5}$, and is inconsistent with A_{ref} by eleven times the mutual standard uncertainty. The fact that all these three values not plotted in Fig. 2b are systematically higher than A_{ref} should not dissuade from the conclusion that A_{ref} for argon is highly reliable.]

3.1.2 Nitrogen

The nitrogen isotherm at 1542 nm is plotted in Fig. 3a, and shown in the literature context by the dispersion plot of Fig. 3b. For nitrogen, there is no high accuracy measurement of static polarizability. Therefore, (1) uses the older capacitance

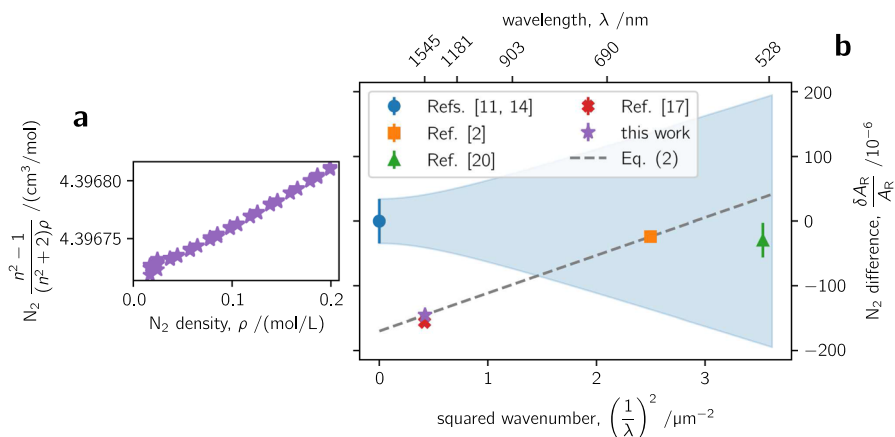


Fig. 3 (a) Single-isotherm results for nitrogen at 1542 nm and 303 K. (b) Dispersion analysis is plotted as relative difference from the reference value; the shaded area is an estimate of uncertainty on the reference value. Errorbars span the uncertainty of the cited literature, which in some cases are smaller than the markers

measurement of Schmidt and Moldover [11] for $A_e(0)$. The *ab initio* estimate of dispersion [13] is not metrology-grade, so $\Delta A_e(\omega)$ uses a Cauchy equation derived from the dipole oscillator strength distributions (DOSD) of Kumar and Meath [14]. Last, a handbook [15] value is used for A_μ , which is based on measurements from 100 years ago [16]. Obviously, this particular reference value synthesis for nitrogen is not well known, and has combined uncertainties of $3.5 \times 10^{-5} \cdot A_e$ [11] plus 1% on the first Cauchy coefficient [14]; the diamagnetic susceptibility is unlikely to affect optical and dielectric comparisons at more than the $4 \times 10^{-6} \cdot A_R$ level.

Though nitrogen data are scarce, Fig. 3b suggests the formulated reference value is erroneous. As stated at the outset, this work and Ref. [2] have been produced with the same apparatus—identical instrumentation for $n - 1$, p , and T_{90} , with the only difference being the wavelength of the laser interrogating the cavity. It is plausible that the same apparatus operated at two widely separated wavelengths should produce a reliable estimate of nitrogen dispersion. Based on the argon result above (see Fig. 2b), it is also plausible that this apparatus should establish an absolute value of nitrogen's molar refractivity within the stated $3 \times 10^{-6} \cdot A_R$ uncertainty. Therefore, one might reasonably formulate a new A_R recommendation based on two measurements from the same apparatus. The results of this work and Ref. [2] both operated at 303 K, and are satisfied by

$$A_R = a_e \left[1 + a_2 \left(\frac{\mu\text{m}}{\lambda} \right)^2 + a_4 \left(\frac{\mu\text{m}}{\lambda} \right)^4 + a_6 \left(\frac{\mu\text{m}}{\lambda} \right)^6 + a_m \right], \quad (2)$$

with the static value equivalent $a_e = 4.386921(20) \text{ cm}^3/\text{mol}$. The λ is vacuum wavelength. The $a_2 = 5.3247(29) \times 10^{-3}$ is larger than the DOSD [14] by 1.2%, which is slightly larger than the DOSD estimate of uncertainty on that Cauchy coefficient. The $a_4 = 3.610 \times 10^{-5}$ and $a_6 = 2.753 \times 10^{-7}$ are fixed values taken from the DOSD. The $a_m = -1.1(1) \times 10^{-5}$ is from the handbook value [15] for magnetic susceptibility. All numbers in parentheses indicate standard uncertainty. Identification of the static value is inhibited by uncertainty in a_m . Between 1542 nm and 633 nm, the recommendation should be accurate within $3 \times 10^{-6} \cdot A_R$. The uncertainty will increase as $\frac{1}{\lambda^2}$, so extrapolation to 532 nm should not incur error greater than $6 \times 10^{-6} \cdot A_R$.

It is emphasized that the recommendation of (2) only harmonizes the two data-points from a single apparatus operated at 633 nm and 1542 nm. Crucially, however, the recommendation is independently supported by Silander et al. [17], whose recent result at 1550.14 nm agrees with (2) within 2.5 times mutual standard uncertainty. Moreover, the dispersion trend of (2) nominally agrees with the spectral lamp measurement of Peck and Khanna [18]. Between the wavelengths 633 nm and 1542 nm, (2) differs from the Sellmeier equation of Peck and Khanna by only $-1.3 \times 10^{-5} \cdot A_R$. Peck and Khanna have no explanation of uncertainty: they state the absolute value of refractivity was “considered significant only to about four digits” and that a refractivity ratio would be “perhaps two orders of magnitude” more accurate than the absolute value. The first statement might mean $4 \times 10^{-4} \cdot A_R$ on the absolute value. The Peck and Khanna absolute value is $1.6 \times 10^{-4} \cdot A_R$ higher than (2) at 633 nm, so within their estimated uncertainty. However, if their ratio

uncertainty is interpreted as $4 \times 10^{-6} \cdot A_R$, it does not cover divergence from (2) for widely separated wavelengths. The divergence of Peck and Khanna might be explained as a chromatic error in their apparatus, which also appears in the dispersion measurement of argon by Peck and Fisher [19]. For argon, between the wavelengths 633 nm and 1542 nm, the *ab initio* Cauchy equation [8] differs from Peck and Fisher's Sellmeier equation by $-1.4 \times 10^{-5} \cdot A_R$. So, the Peck dispersion measurements for nitrogen and argon both exhibit similar deviation in sign and magnitude from modern, independent estimates.

Elsewhere in Fig. 3b: Schmidt and Moldover's [11] nitrogen measurement is $1.7 \times 10^{-4} \cdot A_e$ higher than (2), which is discrepancy at five times mutual standard uncertainty. The inconsistency of Schmidt and Moldover's [11] nitrogen measurement with an updated reference value is not surprising: as mentioned in the previous subsection, their apparatus also produced a high value for argon. The updated formulation of (2) is marginally discrepant with the 532.255 nm value of Kameche [20] by 2.4 times the mutual standard uncertainty. Finally, not shown in Fig. 3b is a refractivity measurement at 800 nm due to Zhang et al. [12], which is discrepant with (2) by three times the mutual standard uncertainty. (Like their argon measurement, Zhang et al. report a nitrogen value higher than this work.)

Compared to argon, nitrogen lacks a dielectric constant measurement of the same caliber as Gaiser and Fellmuth [9], and has no *ab initio* dispersion check. Nevertheless, the present work combined with Silander et al. [17] has established nitrogen on a firmer footing than previously. In the context of the optical pressure scale $p \approx \frac{2RT}{3A_R}(n-1)$, consensus knowledge on the key parameter is at the level of $1.1 \times 10^{-5} \cdot A_R$.

3.2 Discussion about H₂O and D₂O

For water at 373 K, measurement uncertainty in the molar refractivity is dominated by performance of the calibrated pressure transducers, as detailed in Ref. [3]. Operating at 1542 nm incurs no additional uncertainty, and the combined standard uncertainty is $4.1 \times 10^{-4} \cdot A_R$. One uncertainty component that is wavelength dependent is the end-effect error ϵ_ϕ caused by the moisture-dependent reflection phase shift. The ϵ_ϕ was fully characterized at 633 nm. The change in ϵ_ϕ at 1542 nm was estimated by the mirror stack model [21]. The model predicted that ϵ_ϕ decreases by 4.8% at 1542 nm relative to 633 nm. This estimate assumes the same amount of water adsorbs into the coating at both wavelengths, but the model accounts for dispersion of the three materials involved: high and low index layers of the stack and the condensed water in the voids. The results at 1542 nm have had the 4.8% reduction applied to ϵ_ϕ . At 373 K, $\epsilon_\phi \lesssim -0.5$ nm, and a 4.8% change only affects the single-isotherm result at the level of $2 \times 10^{-5} \cdot A_R$.

The single-isotherm results for ordinary and heavy water at 1542 nm and 373 K are plotted in Fig. 4a and Fig. 5a. Imprecision increases at lower density owing to the performance of the calibrated pressure transducers. The single-isotherm water values for A_R in Table 1 use the weighted mean of the data in Figs. 4a and 5a. The

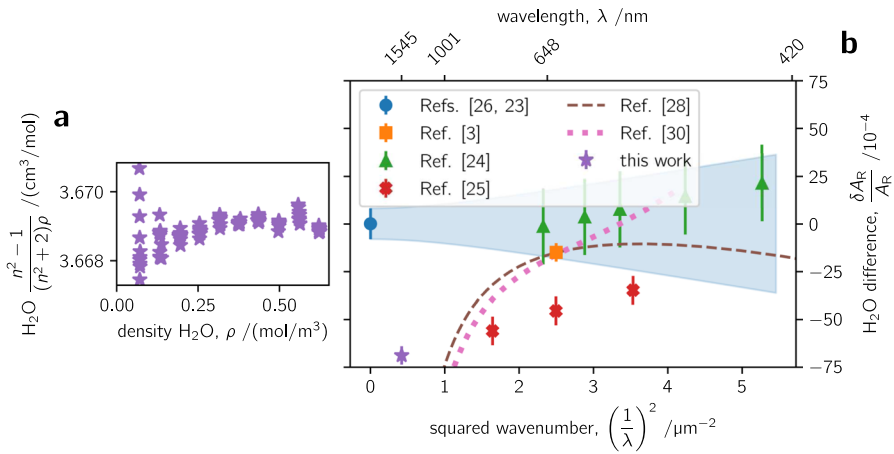


Fig. 4 (a) Single-isotherm results for ordinary water at 1542 nm and 373 K. (b) Dispersion analysis is plotted as relative difference from the reference value; the shaded areas are a rough estimate of standard uncertainty on the reference value. Errorbars span the standard uncertainty of each literature source

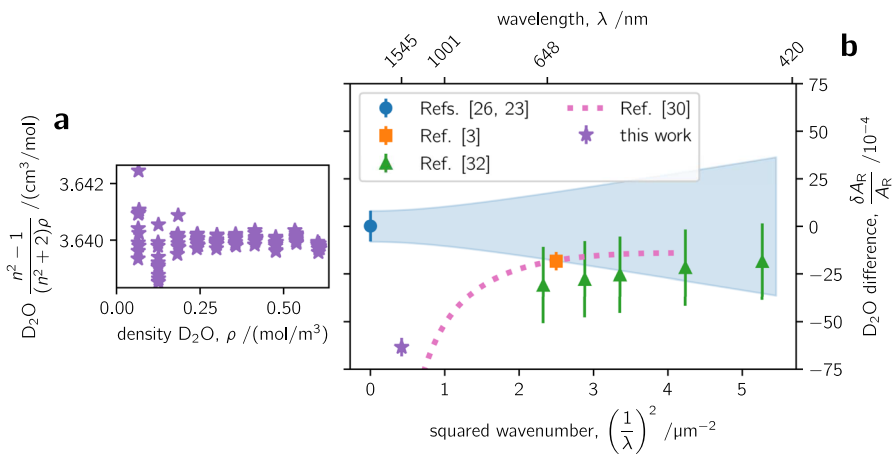


Fig. 5 (a) Single-isotherm results for heavy water at 1542 nm and 373 K. (b) Dispersion analysis is plotted as relative difference from the reference value; the shaded areas are a rough estimate of standard uncertainty on the reference value. Errorbars span the standard uncertainty of each literature source

A_R at 1542 nm appear the only gaseous measurements to date in the near-infrared. The problem of formulating a reference value to compare visible, near-infrared, and zero frequency estimates of A_R is discussed next.

3.2.1 Problems Formulating A_{ref}

Ordinary water has two absorption peaks [22] in the vicinity of 1542 nm: a weak one at 1460 nm and a strong one at 1930 nm. These features preclude the construction of a metrology-grade estimate of $\Delta A_{\epsilon}(\omega)$.

The Cauchy equation for H_2O derived from the DOSD [23] is nominally consistent with visible wavelength measurements [24, 25]. However, a Cauchy equation based on the DOSD is inadequate to describe spectral behavior in the presence of absorption. Typically, for absorbing liquids, terms proportional to λ^{2m} are added to the Cauchy equation (m is an integer). This work at 1542 nm operates at a saddle-point between two absorption peaks, so any smooth interpolating function is likely to be imprecise. For example, Bertie and Lan [22] derived the real refractive index of liquid H_2O by performing the Kramers–Kronig transformation on absorption data. Fitting their data in the range ($667 < \lambda < 1600$) nm with $c_0 + \frac{c_1}{\lambda^2} - c_2\lambda^2$ failed to follow the oscillatory behavior. Between 1400 nm and 1600 nm, error from the fit had a full-range deviation of 0.1 %.

Besides the difficulty of smoothly interpolating A_{R} between two measurements in the same apparatus, a Cauchy equation with λ^2 proportionality would not allow comparison with *ab initio* calculation of electronic polarizability. So, the canonical functions available for $\Delta A_{\epsilon}(\omega)$ do not facilitate accurate comparison of static, near-infrared, and visible wavelength estimates of A_{R} . The compromise of this work uses the following for (1): the $A_{\epsilon}(0)$ from the *ab initio* calculations of Garberoglio et al. [26], the $\Delta A_{\epsilon}(\omega)$ from the DOSD of Zeiss and Meath [23], and the recommendation of Harvey et al. [27] for A_{μ} . (Note that the DOSD of Zeiss and Meath is for H_2O , and this work uses the same dispersion polarizability for H_2O and D_2O .)

The dispersion plots of Figs. 4b and 5b clearly show the shortcoming of the compromise implemented for (1). The result at 1542 nm disagrees with (1) by about $7.5 \times 10^{-3} \cdot A_{\text{R}}$, or nine times mutual standard uncertainty. To be clear, the conclusion of Ref. [3] still stands: the refractivity measurement at 633 nm is consistent with the recent *ab initio* calculation [26], using the DOSD to adjust to zero frequency. Furthermore, the measurement technique of Ref. [3] and the present work is single-wavelength interferometry, and oscillatory behavior caused by absorption has no influence on the accuracy of a refractivity measurement or the deduction of A_{R} . These contradictory statements—that the measurements are accurate and significantly disagree with a reference value—stem from the inadequacy of the reference value in the near-infrared. The contradiction is somewhat allayed by looking at the dispersion of liquid water, as discussed next.

3.2.2 Dispersion of Water

For ordinary water, there are two liquid water dispersion functions plotted in Fig. 4b. One is derived from the IAPWS formulation [28], which is heavily weighted by the classical liquid dispersion of Tilton and Taylor [29]. The IAPWS formulation has a λ^2 proportional term, and extends to wavelengths longer than the 707 nm cutoff of Tilton and Taylor. For Fig. 4b, the average value of the IAPWS (vapor) formulation

at 373 K has been decreased by 1.63 % to intersect with Ref. [3]. Also plotted in Fig. 4b is a more recent liquid measurement by Kedenburg et al. [30], which was performed at 293 K and covered wavelengths ($500 < \lambda < 1600$) nm. The Cauchy equation derived by Kedenburg et al. also has a λ^2 proportional term. The trend of Kedenburg et al. in Fig. 4b has been increased by 1.27 % to intersect with Ref. [3].

Both the liquid dispersion curves in Fig. 4b generally support a feature of the present work: a deviation from $\frac{1}{\lambda^2}$ proportionality compared to other visible measurements of gaseous H₂O [24, 25]. However, both liquid dispersion functions have a λ^2 proportionality too strong to intersect the measurement at 1542 nm. This aspect is probably influenced by the strong absorption peak 1930 nm. The Kramers–Kronig dispersion relation predicts that $n(\lambda)$ decreases as an absorption peak is approached from short wavelength. The IAPWS formulation is mostly constructed from wavelength data shorter than the strong absorption peak; Kedenburg et al. have data extending no further than 1600 nm. Therefore, both liquid Cauchy equations are likely to be driven to a low value of $n(1542\text{ nm})$ by the influence of the 1930 nm absorption on the λ^2 term. The influence of absorption on refractive index is further discussed in App. B.

Heavy water has weak absorption at 1340 nm and 1620 nm, and a strong absorption at 1970 nm [31]. The absorbance at 1970 nm is about five times smaller than the equivalent feature in ordinary water. The liquid dispersion function plotted in Fig. 5b is from the measurement of Kedenburg et al. at 293 K, and has been increased in absolute value by 1.33 % to intersect with Ref. [3]. Again, the liquid dispersion curve helps place the measurement at 1542 nm in context. The departure from the $\frac{1}{\lambda^2}$ proportionality of visible wavelength measurement [32] is expected because of the strong absorption at 1970 nm.

In any case, the two measurements produced by this apparatus have an estimated uncertainty of $4.1 \times 10^{-4} \cdot A_R$. The $7 \times 10^{-3} \cdot A_R$ deviation of the result at 1542 nm from a reference value is a shortcoming of the reference value, and is not likely a problem in measurement [3] or calculation [26].

4 Conclusion

This article was the final installment to a three-part $n(p, T_{90})$ series. The final installment has reported single-isotherm results for argon, nitrogen, ordinary water, and heavy water at the wavelength of 1542 nm. When combined with information from the first two articles [2, 3] which operated at 633 nm, the present work offered insights into dispersion polarizability.

The results have been placed in the literature context of a reference value for the respective molar refractivities. The results indicate that knowledge of the optical properties of argon is highly accurate (~ 3 parts in 10^6) and nitrogen is almost as good (~ 1 part in 10^5). The argon and nitrogen results will help establish the optical pressure scale [1] on a solid metrological foundation for telecom wavelength.

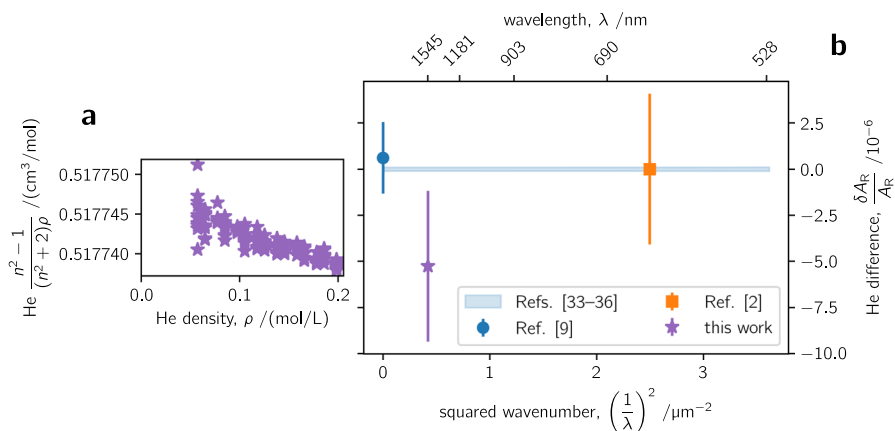


Fig. 6 (a) Single-isotherm results for helium at 1542 nm and 303 K. (b) Dispersion analysis plotted as relative difference from the reference value; the shaded area is an estimate of uncertainty on the *ab initio* reference value. Errorbars span the uncertainty of the cited literature

For water vapor, absorption features in the near-infrared make it difficult to relate the 1542 nm result to either the measurement at 633 nm or the *ab initio* calculation of static electronic polarizability. Nevertheless, the result might help establish a more accurate reference formulation in the C-band infrared—the extant formulation [28] has no gaseous input data in the near-infrared.

Appendix 1: Helium Dispersion, or Cavity Recalibration

Simultaneous and synchronous two-wavelength measurement of helium is a future interest: the cavity compressibility κ cancels, the refractometer becomes truly absolute, and a thermodynamic quantity is realized in a primary way. It might be called “dispersion gas thermometry.” This development awaits dichroic optics coupling to the cavity and, crucially, better knowledge about mirror phase shift—the parameters ϵ_τ and ν_c in the master equation [2].

For now, the apparatus has produced a helium isotherm at 1542 nm, separated in time by 18 months from the isotherms at 633 nm [2]. The result is plotted in Fig. 6a, and its relation to literature is in subplot (b). For helium, all contributors to the reference value of (1) are based on *ab initio* calculation. The $A_e(0)$ is from Puchalski et al. [33], the $\Delta A_e(\omega)$ is from Puchalski et al. [34] with its small correction [35], and the A_μ is from Puchalski et al. [36]. The estimate of uncertainty in calculation is below $10^{-7} \cdot A_R$ at all wavelengths.

For the measurement results in Fig. 6b: The static measurement is due to the highly accurate capacitance measurement of Gaiser and Fellmuth [9]. This is a true absolute measurement, in which apparatus distortion was corrected by mechanical knowledge of elastic properties. The result plotted at 633 nm is not absolute: it is from the present apparatus, in which the cavity compressibility κ was assigned a value [2] that drove $\delta A_R \rightarrow 0$. By contrast, the measurement result

$A_R = 0.5177474(21) \text{ cm}^3/\text{mol}$ plotted at 1542 nm is also from this apparatus, and uses the κ originally estimated at 633 nm. There are two possible interpretations of the optical measurements in Fig. 6b. The first interpretation would be that κ is stable and reproducible within $1.4 \times 10^{-4} \cdot \kappa$ over 18 months and with disassembly and remounting on the wire suspension. (Recall, standard uncertainty for the calibration of compressibility via helium refractivity was estimated to be $1.3 \times 10^{-4} \cdot \kappa$.) The second interpretation is that two measurements at 633 nm and 1542 nm have validated the *ab initio* calculation of dispersion polarizability [34] within the $4 \times 10^{-6} \cdot A_R$ precision of the apparatus.

Finally, the first interpretation above brings the question: which estimate of κ to use? This work used the *old* value of κ , reasoning that cavity compressibility does not change with time, and a constant systematic error in the apparatus would give a more reliable estimate of dispersion in argon and nitrogen. If the refractometer were updated to the new value for κ , the molar refractivity values at 1542 nm in Table 1 would decrease by $0.7 \times 10^{-6} \cdot A_R$.

Molecular Absorption and Refractive Index

The Beer–Lambert law describes light absorption $I = I_0 \exp(-\mu d)$ as an exponential decrease in transmitted intensity I through a (gas) medium of pathlength d . The absorption coefficient is given by

$$\mu(\lambda) = \sigma_m(\lambda)\rho_n + \sigma_b(\lambda)\rho_n^2 + \dots \quad (3)$$

Absorption depends on wavelength λ , and ρ_n is number density. The $\sigma_m(\lambda)$ is the monomer absorption cross-section. The $\sigma_b(\lambda)$ is the collision-induced absorption, in which a dipole is created by binary interactions between molecules.

An absorbing medium has a complex refractive index

$$\hat{n} = n + ik, \quad (4)$$

with the optical extinction coefficient k related to the absorption coefficient μ via $k = \mu \frac{\lambda}{4\pi}$. A refractometer measures \hat{n} but theory calculates n (i.e., as electronic polarizability). Consequently, for an absorbing gas, measurement and calculation of refractive index will diverge by $\delta n \equiv \hat{n} - n$. The divergence is given by a Kramers–Kronig transformation

$$\delta n(\lambda) = \frac{2\lambda^2}{\pi} \int_0^\infty \frac{k(\lambda') d\lambda'}{\lambda'(\lambda^2 - \lambda'^2)} \quad (5)$$

on the optical extinction coefficient k . Therefore, knowledge about μ [37, 38] informs the deviation δn [39, 40] between experiment and theory.

The δn result for H₂O is plotted in Fig. 7a, and calculation is referenced to $p = 1 \text{ kPa}$ and $T = 373 \text{ K}$ conditions. The μ was obtained from HITRAN [37, 38] for wavenumbers ($0.0001 < \frac{1}{\lambda} < 2.5$) μm^{-1} . The abscissa of Fig. 7a is linear in wavelength to show the complex behavior in the near-infrared, and two

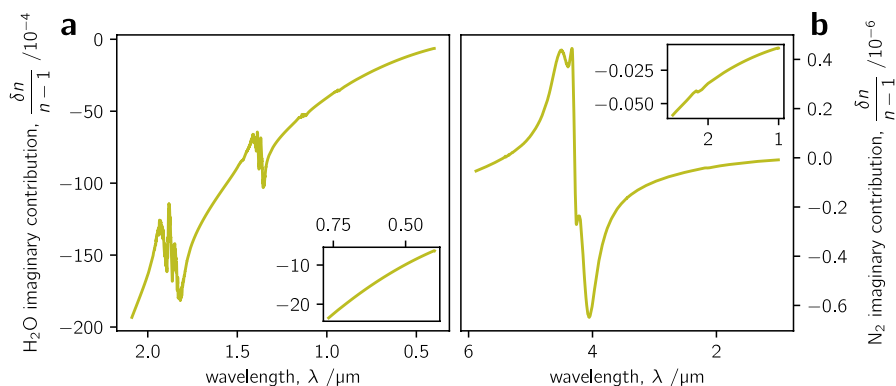


Fig. 7 Contribution of absorption to the refractive index. (a) Ordinary water vapor at 1 kPa and 373 K. The inset shows the contribution at visible wavelength. (b) Nitrogen at 0.5 MPa and 303 K. The inset shows a barely perceptible influence from the overtone at 2.16 μm

interesting features are clear. First, refractive index at 633 nm is already perturbed by the strong infrared absorption. Second, between 633 nm and 1542 nm the fractional deviation $\frac{\delta n}{n-1}$ is about -8×10^{-3} . Referring to Fig. 4b of the main text: the two H_2O datapoints of this apparatus diverge in $\frac{\delta A_R}{A_R}$ proportional to wavelength. A quantitative estimate of this divergence is subjective, but -6×10^{-3} between the two wavelengths is reasonable. The nominal consistency between this subjective estimate and the $\frac{\delta n}{n-1}$ predicted by Fig. 7a is remarkable. [Two notes: best-knowledge $\mu(\lambda)$ does not satisfy the idealized limits of (5), and the $\mu(\lambda)$ employed does not include the water vapor continuum.]

The preceding demonstration with H_2O encourages a prediction of the influence that absorption in nitrogen might have on (2). Nitrogen is a homonuclear molecule without a dipole moment, and does not exhibit a rovibrational absorption spectrum. It has a strong triple bond, which can not be excited by the (low) energy of infrared radiation. Therefore, for wavelengths longer than visible, nitrogen has a $\sigma_m(\lambda)$ near zero. However, nitrogen is active in the infrared by collision-induced absorption. For $\sigma_b(\lambda)$ in (3), the HITRAN database is again the relevant resource [41]. For ρ_n at ambient conditions the resulting μ is weak, but the fundamental band is at 4.3 μm , and an overtone at 2.16 μm is close to telecom wavelength. However, the Kramers–Kronig transformation reveals δn to be a very small effect for telecom wavelengths, as shown in Fig. 7b. So, nitrogen absorption should not cause imprecision larger than $10^{-7} \cdot A_R$ in (2)—for example, if optical refractivity were compared to dielectric constant.

Supplementary Information The online version contains supplementary material available at <https://doi.org/10.1007/s10765-024-03412-5>.

Acknowledgments The need to accurately establish A_R at 1542 nm for argon and nitrogen was recognized in 2018, and formed one-third part of a collaborative research and development agreement between

NIST and Fluke Calibration. The agreement was CN-18-0133, and Robert Haines was the co-principal investigator at Fluke Calibration.

Author Contributions Investigation: PFE; Validation: YY.

Funding Work undertaken as part of the authors' duties fulfilling the mission of their institutes.

Open Access This article is licensed under a Creative Commons Attribution 4.0 International License, which permits use, sharing, adaptation, distribution and reproduction in any medium or format, as long as you give appropriate credit to the original author(s) and the source, provide a link to the Creative Commons licence, and indicate if changes were made. The images or other third party material in this article are included in the article's Creative Commons licence, unless indicated otherwise in a credit line to the material. If material is not included in the article's Creative Commons licence and your intended use is not permitted by statutory regulation or exceeds the permitted use, you will need to obtain permission directly from the copyright holder. To view a copy of this licence, visit <http://creativecommons.org/licenses/by/4.0/>.

References

1. K. Jousten, A unit for nothing. *Nat. Phys.* **15**, 618 (2019). <https://doi.org/10.1038/s41567-019-0530-8>
2. P.F. Egan, Y. Yang, Optical $n(p, T_{90})$ measurement suite 1: He, Ar, and N_2 . *Int. J. Thermophys.* **44**, 181 (2023). <https://doi.org/10.1007/s10765-023-03291-2>
3. P.F. Egan, Y. Yang, Optical $n(p, T_{90})$ measurement suite 2: H_2O and D_2O . *Int. J. Thermophys.* **45**, 89 (2024). <https://doi.org/10.1007/s10765-024-03380-w>
4. P. Egan, E. Stanfield, J. Stoup, C. Meyer, Conversion of a piston-cylinder dimensional dataset to the effective area of a mechanical pressure generator. *NCSLI Meas.* **15**, 26–43 (2023) https://tsapps.nist.gov/publication/get_pdf.cfm?pub_id=935867
5. C. Gaiser, B. Fellmuth, R.M. Gavioso, M. Kalemci, V. Kytin, T. Nakano, A. Pokhodun, P.M.C. Rourke, R. Rusby, F. Sparasci, P.P.M. Steur, W.L. Tew, R. Underwood, R. White, I. Yang, J. Zhang, 2022 update for the differences between thermodynamic temperature and ITS-90 below 335 K. *J. Phys. Chem. Ref. Data* **51**, 043105 (2022). <https://doi.org/10.1063/5.0131026>
6. G. Garberoglio, A.H. Harvey, Path-integral calculation of the second dielectric and refractivity virial coefficients of helium, neon, and argon. *J. Res. Natl Inst. Stand. Technol.* **125**, 125022 (2020). <https://doi.org/10.6028/jres.125.022>
7. P.M.C. Rourke, C. Gaiser, B. Gao, M.R. Moldover, L. Pitre, D. Madonna Ripa, R.J. Underwood, Refractive-index gas thermometry. *Metrologia* **56**, 032001 (2019). <https://doi.org/10.1088/1681-7575/ab0dbe>
8. M. Lesiuk, B. Jeziorski, First-principles calculation of the frequency-dependent dipole polarizability of argon. *Phys. Rev. A* **107**, 042805 (2023). <https://doi.org/10.1103/PhysRevA.107.042805>
9. C. Gaiser, B. Fellmuth, Polarizability of helium, neon, and argon: new perspectives for gas metrology. *Phys. Rev. Lett.* **120**, 123203 (2018). <https://doi.org/10.1103/PhysRevLett.120.123203>
10. M. Lesiuk, B. Jeziorski, Diamagnetic susceptibility of neon and argon including leading relativistic effects. *Phys. Rev. A* **109**, 012820 (2024). <https://doi.org/10.1103/PhysRevA.109.012820>
11. J.W. Schmidt, M.R. Moldover, Dielectric permittivity of eight gases measured with cross capacitors. *Int. J. Thermophys.* **24**, 375–403 (2003). <https://doi.org/10.1023/A:1022963720063>
12. J. Zhang, Z.H. Lu, L.J. Wang, Precision refractive index measurements of air, N_2 , O_2 , Ar, and CO_2 with a frequency comb. *Appl. Opt.* **47**, 3143–3151 (2008). <https://doi.org/10.1364/AO.47.003143>
13. C. Jamorski, M.E. Casida, D.R. Salahub, Dynamic polarizabilities and excitation spectra from a molecular implementation of time-dependent density-functional response theory: N_2 as a case study. *J. Chem. Phys.* **104**, 5134–5147 (1996). <https://doi.org/10.1063/1.471140>
14. A. Kumar, W.J. Meath, Constrained anisotropic dipole oscillator strength distribution techniques, and reliable results for anisotropic and isotropic dipole molecular properties, with applications to H_2 and N_2 . *Theor. Chim. Acta* **82**, 131–152 (1992). <https://doi.org/10.1007/BF01113134>

15. W.M. Haynes (ed.), *CRC Handbook of Chemistry and Physics*, 95th edn (CRC Press, Boca Raton, 2014). <https://doi.org/10.1201/b17118>
16. L.G. Hector, The magnetic susceptibility of helium, neon, argon, and nitrogen. *Phys. Rev.* **24**, 418–425 (1924). <https://doi.org/10.1103/PhysRev.24.418>
17. I. Silander, J. Zakrisson, O. Axner, M. Zelan, Realization of the pascal based on argon using a Fabry–Perot refractometer. *Opt. Lett.* **49**, 3296–3299 (2024). <https://doi.org/10.1364/OL.523293>
18. E.R. Peck, B.N. Khanna, Dispersion of nitrogen. *J. Opt. Soc. Am.* **56**, 1059–1063 (1966). <https://doi.org/10.1364/JOSA.56.001059>
19. E.R. Peck, D.J. Fisher, Dispersion of argon. *J. Opt. Soc. Am.* **54**, 1362–1364 (1964). <https://doi.org/10.1364/JOSA.54.001362>
20. M. Kameche, Réfractométrie absolue basée sur l'hélium. Ph.D. thesis, Conservatoire National des Arts et Metiers, Paris (2013). <https://dumas.ccsd.cnrs.fr/dumas-01700756>
21. T.A. Germer, pySCATMECH: a Python interface to the SCATMECH library of scattering codes, in *Reflection, Scattering, and Diffraction from Surfaces VII* (SPIE, 2020), **11485**, 43–54 <https://doi.org/10.1117/12.2568578>
22. J.E. Bertie, Z. Lan, Infrared intensities of liquids XX: the intensity of the OH stretching band of liquid water revisited, and the best current values of the optical constants of H₂O(l) at 25 °C between 15,000 and 1 cm⁻¹. *Appl. Spectrosc.* **50**, 1047–1057 (1996). <https://doi.org/10.1366/0003702963905385>
23. G. Zeiss, W.J. Meath, The H₂O–H₂O dispersion energy constant and the dispersion of the specific refractivity of dilute water vapour. *Mol. Phys.* **30**, 161–169 (1975). <https://doi.org/10.1080/00268977500101841>
24. C. Cuthbertson, M. Cuthbertson, On the refraction and dispersion of the halogens, halogen acids, ozone, steam, oxides of nitrogen and ammonia. *Philos. Trans. R. Soc. Lond. A* **213**, 1–26 (1914). <https://doi.org/10.1098/rsta.1914.0001>
25. R. Schödel, A. Walkov, A. Abou-Zeid, High-accuracy determination of water vapor refractivity by length interferometry. *Opt. Lett.* **31**, 1979–1981 (2006). <https://doi.org/10.1364/OL.31.001979>
26. G. Garberoglio, C. Lissoni, L. Spagnoli, A.H. Harvey, Comprehensive quantum calculation of the first dielectric virial coefficient of water. *J. Chem. Phys.* **160**, 024309 (2024). <https://doi.org/10.1063/5.0187774>
27. A.H. Harvey, J. Hrubý, K. Meier, Improved and always improving: reference formulations for thermophysical properties of water. *J. Phys. Chem. Ref. Data* **52**, 011501 (2023). <https://doi.org/10.1063/5.0125524>
28. A.H. Harvey, J.S. Gallagher, J.M.H. Levelt Sengers, Revised formulation for the refractive index of water and steam as a function of wavelength, temperature and density. *J. Phys. Chem. Ref. Data* **27**, 761–774 (1998). <https://doi.org/10.1063/1.556029>
29. L.W. Tilton, J.K. Taylor, Refractive index and dispersion of distilled water for visible radiation, at temperatures 0 to 60 °C. *J. Res. Natl. Bur. Stand.* **20**, 419 (1938). <https://doi.org/10.6028/jres.020.024>
30. S. Kedenburg, M. Vieweg, T. Gissibl, H. Giessen, Linear refractive index and absorption measurements of nonlinear optical liquids in the visible and near-infrared spectral region. *Opt. Mater. Express* **2**, 1588–1611 (2012). <https://doi.org/10.1364/OME.2.001588>
31. J.G. Bayly, V.B. Kartha, W.H. Stevens, The absorption spectra of liquid phase H₂O, HDO and D₂O from 0.7 μm to 10 μm. *Infrared Phys.* **3**, 211–222 (1963). [https://doi.org/10.1016/0020-0891\(63\)90026-5](https://doi.org/10.1016/0020-0891(63)90026-5)
32. C. Cuthbertson, M. Cuthbertson, The refractive index of gaseous heavy water. *Proc. R. Soc. Lond. A* **155**, 213–217 (1936). <https://doi.org/10.1098/rspa.1936.0094>
33. M. Puchalski, K. Szalewicz, M. Lesiuk, B. Jeziorski, QED calculation of the dipole polarizability of helium atom. *Phys. Rev. A* **101**, 022505 (2020). <https://doi.org/10.1103/PhysRevA.101.022505>
34. M. Puchalski, K. Piszczatowski, J. Komasa, B. Jeziorski, K. Szalewicz, Theoretical determination of the polarizability dispersion and the refractive index of helium. *Phys. Rev. A* **93**, 032515 (2016). <https://doi.org/10.1103/PhysRevA.93.032515>
35. K. Pachucki, M. Puchalski, Refractive index and generalized polarizability. *Phys. Rev. A* **99**, 041803 (2019). <https://doi.org/10.1103/PhysRevA.99.041803>
36. M. Puchalski, M. Lesiuk, B. Jeziorski, Relativistic treatment of the diamagnetic susceptibility of helium. *Phys. Rev. A* **108**, 042812 (2023). <https://doi.org/10.1103/PhysRevA.108.042812>

37. R. Kochanov, I. Gordon, L. Rothman, P. Weislo, C. Hill, J. Wilzewski, HITRAN application programming interface (HAPI): A comprehensive approach to working with spectroscopic data. *J. Quant. Spectrosc. Radiat. Transf.* **177**, 15–30 (2016). <https://doi.org/10.1016/j.jqsrt.2016.03.005>
38. I. Gordon et al., The HITRAN2020 molecular spectroscopic database. *J. Quant. Spectrosc. Radiat. Transf.* **277**, 107949 (2022). <https://doi.org/10.1016/j.jqsrt.2021.107949>
39. K. Ohta, H. Ishida, Comparison among several numerical integration methods for Kramers–Kronig transformation. *Appl. Spectrosc.* **42**, 952–957 (1988). <https://doi.org/10.1366/0003702884430380>
40. M.J. Müller, F. Dobener. pyElli: a numerical solver for spectral ellipsometry (2024). <https://doi.org/10.5281/zenodo.5702469>
41. T. Karman et al., Update of the HITRAN collision-induced absorption section. *Icarus* **328**, 160–175 (2019). <https://doi.org/10.1016/j.icarus.2019.02.034>

Publisher's Note Springer Nature remains neutral with regard to jurisdictional claims in published maps and institutional affiliations.